

Method for the in situ preparation of a single layer of zeolite Beta crystals on a molybdenum substrate for microreactor applications

M.J.M. Mies^a, E.V. Rebrov^a, J.C. Jansen^b, M.H.J.M. de Croon^a, J.C. Schouten^{a,*}

^a Department of Chemical Engineering and Chemistry, Eindhoven University of Technology, P.O. Box 513, 5600 MB Eindhoven, The Netherlands

^b Catalysis Engineering, DelftChemTech, Delft University of Technology, Julianalaan 136, 2628 BL Delft, The Netherlands

Received 2 October 2006; revised 30 January 2007; accepted 4 February 2007

Abstract

A method for the hydrothermal synthesis of a single layer of zeolite Beta crystals on a molybdenum substrate for microreactor applications has been developed. Before the hydrothermal synthesis, the surface of the substrate was modified by an etching procedure that increases the roughness at the nanoscale level without completely eliminating the surface lay structure. Then, thin films of Al₂O₃ (170 nm) and TiO₂ (50 nm) were successively deposited by atomic layer deposition (ALD) on the substrate. The internal Al₂O₃ film protects the Mo substrate from oxidation up to 550 °C in an oxidative environment. The high wettability of the external TiO₂ film after UV irradiation increases zeolite nucleation on its surface. The role of the metal precursor (TiCl₄ vs TiI₄), deposition temperature (300 vs 500 °C), and film thickness (50 vs 100 nm) was investigated to obtain titania films with the slowest decay in the superhydrophilic behavior after UV irradiation. Zeolite Beta coatings with a Si/Al ratio of 23 were grown at 140 °C for 48 h. After ion exchange with a 10⁻⁴ M cobalt acetate solution, the activity of the coatings was determined in the ammoxidation of ethylene to acetonitrile in a microstructured reactor. A maximum reaction rate of 220 μmol C₂H₃N g⁻¹ s⁻¹ was obtained at 500 °C, with 42% carbon selectivity to acetonitrile.

© 2007 Elsevier Inc. All rights reserved.

Keywords: Zeolite Beta; In situ synthesis; Thin zeolitic coatings; Molybdenum; Atomic layer deposition; Surface roughness; Surface hydrophilicity; Protective coatings; Microreactor; Ethylene ammoxidation; Acetonitrile

1. Introduction

Three-dimensional large-pore zeolite Beta (BEA) is currently applied in various catalytic gas- and liquid-phase processes; important examples include the fluid catalytic cracking and dewaxing of petroleum oils [1], alkylation and acylation of aromatics [2,3], isomerization of alkanes [4], Fischer–Tropsch synthesis of iso-paraffins [5], deNO_x [6,7], selective hydrogenations [8,9], and ammoxidation of light paraffins and olefins [10]. Besides these large-scale processes, zeolite Beta also is applied in the synthesis of fine chemicals [3]. Extrudates of zeolite Beta, consisting of zeolite crystals and a binder material, are often applied, resulting in low catalyst efficiency [11]. Application of zeolitic coatings improves catalyst performance, as demonstrated in the case of membrane reactors [12], distilla-

tion units [13], catalytic packings [14,15], monoliths [16], and deNO_x reactors [17].

Fast catalytic reactions involving large heat effects can be further intensified when carried out over zeolitic coatings up to 5 μm thick grown directly in the channels of a microstructured reactor, fabricated in a metal substrate [18,19]. The highly exothermic ammoxidation of ethylene to acetonitrile over zeolite Beta coatings exemplifies such reactions. The large geometrical surface area of the channel walls provides a large interface area between the reactants and the coating. The absence of both binder and macropores improves mass transfer in the coating [11,18]. Heat transfer is enhanced by the chemical bonds between the coating and the substrate, as well as the higher apparent density of the coating [20]. Therefore, methods need to be developed and optimized for the deposition of thin zeolitic coatings on the metal substrate. The hydrothermal synthesis method is an elegant way to grow a single layer of zeolite crystals directly in microchannels [18,19,21].

* Corresponding author.

E-mail address: j.c.schouten@tue.nl (J.C. Schouten).

Molybdenum is often chosen as a substrate material for microreactor applications due to its high thermal conductivity and mechanical stability [22–24]. Above 350 °C in the presence of oxygen, molybdenum oxidizes to orthorhombic MoO₃ [25]. Furthermore, molybdenum dissolves during the in situ growth of zeolitic coatings in the highly alkaline synthesis mixture [23]. Therefore, an approach to developing Mo-based (micro-)structured devices is to use the intrinsic properties of molybdenum through the application of thin protective films on the metal surface [25–28]. Both chemical [29,30] and structural [31,32] properties of the substrate surface, as well as its wettability, are of importance to in situ zeolite growth. The surface roughness affects zeolite growth as well as bonding of zeolite crystals with the substrate. A roll casting process used for metal foil production usually produces a surface with lay (i.e., the predominant direction of the surface texture). Striations or peaks and valleys on a metal foil are usually observed in the direction in which the tool was drawn across the surface. The presence of lay is an important factor in the hydrophilic properties of a surface.

Substrate wettability can be improved by surface treatments [33,34] or by deposition of a hydrophilic film [23]; for example, a titania film can be made superhydrophilic (>15 OH nm⁻²) by UV irradiation [35,36]. Titania thin films, deposited by atomic layer deposition (ALD), have been the subject of extensive research [37–39] due to different applications such as fuel cells, chemical sensors, and photocatalysis. Films that were grown below 140 °C had an amorphous structure, whereas a polycrystalline structure appeared at deposition temperatures above 165 °C regardless of the crystallinity of the substrate [37]. Films grown above 210 °C revealed a polycrystalline anatase structure for a film thickness of 15–55 nm. The influence of the substrate on the TiO₂ film growth has been investigated on substrates including Si [40], KBr [41], soda-lime glass [42], and MgO [43]. In all cases, anatase was formed at 300 °C with no preferred orientation. The deposition of ALD titania films has been focused primarily on using the metal sources titanium chloride, titanium isopropoxide, and titanium ethoxide. Water is the primary non-metal precursor used for titania growth. More recently, titanium iodide has been investigated as a possible precursor [44–46]. Compared with the more common TiCl₄-based ALD process, the TiI₄-based process yields a growth rate about four times higher on α -Al₂O₃ substrates at 600 °C. Furthermore, the TiI₄ process was found to produce films with a higher degree of crystallinity at lower temperatures. Therefore, the advantage of TiI₄ compared with TiCl₄ seems to be its relatively easy ligand release at temperatures above 300 °C. Films grown at 400 and 500 °C had a mixed anatase and rutile crystal structure, with rutile the dominant phase. Precursors and deposition techniques also contribute to the phase formation.

The present study focused on the development of a method for the hydrothermal growth of zeolite Beta coatings with a single layer of crystals on a Mo substrate. First, the surface of the molybdenum substrate was modified before hydrothermal synthesis. Then, synthesis conditions were optimized to yield a perfectly ordered single layer of zeolite Beta crystals. Finally, the activity of the Co-zeolite Beta coatings in the ethylene

ammoxidation to acetonitrile in a microstructured reactor was evaluated.

2. Experimental

2.1. Surface modification of the molybdenum substrate

Experiments were carried out on 10 × 10 mm² and 40 × 10 mm², 100- μ m-thick molybdenum (Aldrich, 99.9+ wt%) substrates. The substrates were boiled in xylene for 1 h to remove organic contaminations, dried at 140 °C for 1 h, and treated by an etching mixture containing 4.3 vol% H₂O₂ (Fluka) and 3.6 vol% NH₄OH (Riedel de Haën) in distilled water. Then aluminum and titanium oxide thin films were successively deposited by ALD on the Mo substrates. The deposition of the films was performed in a flow-type reactor of 0.196 L at a pressure of about 5 mbar. Trimethylaluminum (TMA) was used as the metal precursor for the alumina film, and titanium chloride (TiCl₄) or titanium iodide (TiI₄) was used for the titania film. In all cases, H₂O was used as the oxidant. The H₂O, TMA, TiCl₄, and TiI₄ precursors were stored in reservoirs outside the reactor at 22, 20, 22, and 110 °C, respectively. In the TMA–H₂O and TiCl₄–H₂O processes, precursor pulses of 600 ms were separated by nitrogen pulses of 1200 ms. In the TiI₄–H₂O process, the following pulse sequence was applied: TiI₄ (2500 ms)–N₂ (2500 ms)–H₂O (600 ms)–N₂ (1200 ms). A total of 2431 cycles was required for the deposition of a 170-nm alumina film. The deposition of 50- and 100-nm titania films required a number of 1111 and 2222 cycles, respectively. Before zeolite synthesis, the substrates were UV irradiated for 3 h at room temperature in a metal box (UV lamp: Hanovia 679A-36; 450 W; λ range, 220–1400 nm). Hereinafter, the TiO₂/Al₂O₃/Mo substrate is referred to as the TAMo substrate.

2.2. Zeolite Beta precursor gel

The silica and alumina solutions were prepared separately. The silica solution was prepared by dissolving appropriate amounts of NaCl (Merck), KCl (Merck), and tetraethylammonium hydroxide (TEAOH, 40 wt%, Fluka) in demineralized water, after which colloidal silica (Ludox HS-40, 40 wt% in water) was added. The silica solution was stirred for 0.5 h until the mixture was homogenized. The alumina solution was prepared by dissolving NaOH (Merck) and NaAlO₂ (0.53 wt% Al₂O₃, 0.44 wt% Na₂O, Riedel de Haën) in demineralized water under continuous stirring. Subsequently, the silica solution was slowly added to the alumina solution, after which the mixture was shaken vigorously to prevent formation of a gel. The synthesis mixture was stirred at high speed (600 rpm) for 1 h at room temperature. Gels of the following oxide molar composition were prepared for the synthesis: 1.6 Na₂O:0.93 K₂O:11.4 (TEA)₂O:1 Al₂O₃:46 SiO₂:710 H₂O:1.8 HCl.

2.3. Hydrothermal treatment

Directly after the UV irradiation step, the TAMo substrate was positioned in the synthesis mixture at 20 mm below the

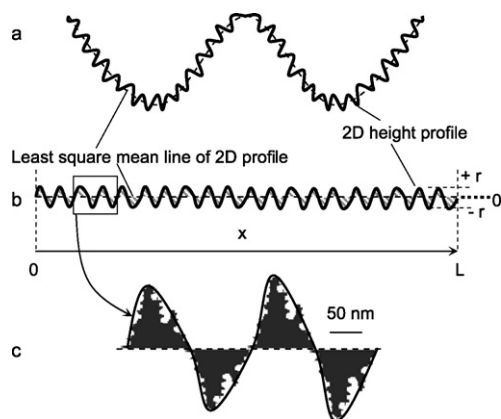


Fig. 1. (a) A 2D surface profile of a substrate showing the intrinsic waviness. (b) The average roughness value, R_a , is calculated from the 2D profile after correction of the waviness. The R_a value is calculated from the integral of the absolute value of the roughness profile (shaded area) divided by the length L (Eq. (1)). (c) The R_a value does not provide information about the surface roughness at the nanoscale level.

gas–liquid interface with $10 \times 10 \text{ mm}^2$ surfaces parallel to the gravity vector. The synthesis was carried out at 140 or 150 °C under autogenic pressure for up to 48 h. A 50-mL PEEK insert filled with 35 mL of solution was positioned in a stainless steel outer shell of the autoclave and closed. In some experiments, the outer shell of the autoclave was preheated to 180 °C to provide rapid heating of the synthesis mixture with an initial heating rate of 10 °C min^{-1} [47]. The zero of synthesis time was taken as the time when the autoclave was placed in a convection oven maintained at the synthesis temperature. The syntheses were performed at static conditions. After the synthesis, the autoclave was quenched in water to room temperature. The zeolite particles from the bottom of the autoclave were filtered through a 0.22- μm filter (Millipore), washed with demineralized water, and dried for 24 h at room temperature.

2.4. Characterization of substrate and coatings

The substrate surface roughness (R_a) was determined by laser scanning confocal microscopy (LSCM). The digitized two-dimensional (2D) surface profile (Fig. 1a) was corrected for the intrinsic waviness of the substrate (Fig. 1b). The average R_a values were determined by Eq. (1) from three 2D height profiles taken at three different locations on the substrate parallel to the direction of the lay of the surface,

$$R_a = \frac{1}{L} \int_0^L |r(x)| dx, \quad (1)$$

where $r(x)$ is the difference between the absolute height and the least squares mean line of the 2D surface profile at position x and L is the total length of the analyzed profile (Fig. 1b). R_a does not include information about the frequency that the height profile crosses the least squares mean line. Furthermore, R_a does not include information about the roughness of the surface at the nanoscale level (Fig. 1c). Therefore, a second parameter was introduced to characterize the surface roughness by

taking the weight loss per area (g m^{-2}) after the etching procedure. For example, a substrate that lost 4 g m^{-2} after etching is referred to as S_4 , whereas the initial substrate is designated S_0 .

Film hydrophilicity was evaluated by contact angle measurements of water on the titania films using an automatic contact angle meter (DataPhysics OCA 30) at a relative humidity of 40%. A 2.0- μL droplet of demineralized water was dropped on the surface of the substrate. The contact angle of the water droplet with the substrate was determined with SCA 20 software before the UV irradiation and 10 and 200 min afterward.

The weight difference of the TAMo substrate before and the TAMo substrate with the zeolitic coating after the hydrothermal synthesis was determined with an analytical mass balance (Mettler Toledo XS105) and used to calculate the zeolite coverage. The Si conversion of the synthesis mixture is defined as

$$\text{Si}_{\text{conversion}} = \frac{\text{mol}(\text{Si}_{\text{powder}} + \text{Si}_{\text{coating}})}{\text{molSi}_{\text{precursor}}} \times 100\%, \quad (2)$$

where the molar amounts of $\text{Si}_{\text{powder}}$ and $\text{Si}_{\text{coating}}$ are calculated from both the as-synthesized zeolite powder and coatings after correction for the amount of water, template, and cations present in the zeolite.

The synthesized coatings were examined by X-ray diffraction (XRD) for phase identification and crystal orientation. XRD data were collected on a Rigaku Geigerflex diffractometer using $\text{CuK}\alpha$ radiation (1.5405 Å). XRD patterns were recorded in the range of 5–50° 2θ using step scanning at 0.02° 2θ per step and a counting time of 4 s for each step. The coating surface coverage and crystal morphology were evaluated by scanning electron microscopy (SEM) using a JEOL JSM-840A microscope and atomic force microscopy using a Spema-B scanning probe microscope with Nova RC1 software. The crystal size distribution and the average crystal size were determined from SEM images of various positions on the surface, where the total number of analyzed crystals was at least 300. The elemental composition of the coatings was analyzed by X-ray photoelectron spectroscopy (XPS) on a VG Escalab MKII spectrometer, equipped with a dual Al/MgK α X-ray source and a hemispherical analyzer with a five-channeltron detector. Spectra were obtained using the aluminium anode ($\text{AlK}\alpha = 1486.6 \text{ eV}$) operating at 250 W and a constant pass energy of 20 eV with a background pressure of 2×10^{-9} mbar. Nitrogen adsorption isotherms were obtained on an ASAP-2020 Micromeritics instrument with a standard procedure after vacuum pretreatment at 300 °C for 12 h up to a residual pressure below 0.1 Pa. The surface area of the zeolitic coating was determined from the nitrogen adsorption–desorption isotherms at -196 °C in the range of relative pressures of 0.001–0.4. The pore size distribution was obtained by the Horvath–Kawazoe method. The full pore volume was calculated from the maximum adsorption value obtained from the N_2 adsorption isotherm.

2.5. Ethylene ammoxidation reaction

The as-synthesized coatings were subjected to a posttreatment procedure consisting of calcination and ion-exchange steps to obtain Co(II)-zeolite Beta coatings. The sequence and

Table 1
Overview of the post-treatment steps used for coating activation

Step no.	Process	Temperature (°C)	Heating rate (°C min ⁻¹)	Medium	Other conditions	Repetition	Dwell (h)
1	Water rinse	r.t.	–	Demi water	–	–	–
2	Ultrasonic treatment	r.t.	–	Demi water	60 Hz, 120 W	–	1
3	Drying	110	–	Air	–	–	12
4	Calcination	295	1	Air	50 mL min ⁻¹	–	2
5	Calcination	500	1	Helium	50 mL min ⁻¹	–	2
6	Ion-exchange	80	–	1 M NH ₄ NO ₃	Reflux cooler, stirring	3	2
7	Water rinse	80	–	Demi water	–	2	0.75
8	Drying	110	–	Demi water	–	–	12
9	Calcination	500	1	Helium	100 mL min ⁻¹	–	2
10	Ion-exchange	80	–	10 ⁻⁴ M cobalt acetate, 200 mL	Reflux cooler, stirring	–	3
11	Water rinse	r.t.	–	Demi water	–	2	–
12	Drying	110	–	Demi water	–	–	12
13	Calcination	295	1	Air	50 mL min ⁻¹	–	2
14	Calcination	500	1	Helium	50 mL min ⁻¹	–	2

conditions of the various treatments are specified in Table 1. XPS analysis on the coatings after the posttreatment resulted in a Si/Al ratio of 23 and a Co/Al ratio of 0.5.

The reaction was carried out in a molybdenum plate-type microreactor. Four coated TAMo substrates with dimensions of 40 × 10 × 0.1 mm³ were inserted in a microstructured reactor at a distance of 350 μm from one another. The reactor was operated in the differential mode [22]. Blank experiments were carried out on inert titanium plates to exclude the contribution of the reactor material to reactant conversion. A total catalyst weight of 0.0018 g was applied for the reaction. The Co-Beta coatings were pretreated in a helium flow of 33 mL min⁻¹ for 1 h at 530 °C. Subsequently, the reactor temperature was decreased to the desired value, and the reactant mixture was introduced at a flow rate of 33 mL min⁻¹ (STP) with a composition of ethylene (2 vol%), ammonia (2 vol%), and oxygen (2 vol%), balanced by helium. The reaction rate and product selectivity were determined under steady-state conditions at 350–500 °C, with a 1-h dwell at each temperature. The concentration of the components in the effluent gas was analyzed with an online Varian micro-gas chromatograph (CP-4900), equipped with a thermal conductivity detector. Helium was used as a carrier gas. The analysis time was 80 s for each injection. N₂, O₂, CH₄, NO, and CO were analyzed on a molsieve 5A column (0.25 mm ID, 10 m) operated at 175 °C and 350 kPa. C₂H₄, C₂H₆, CO₂, NH₃, and H₂O were analyzed on a poraPLOT-U column (0.25 mm i.d., 10 m long) operated at 65 °C and 200 kPa. CH₃CN and CH₃OH were analyzed on a poraPLOT-U column (0.25 mm i.d., 10 m long) operated at 175 °C and 150 kPa. The carbon and nitrogen mass balances were closed within 95%; however, the carbon balance was closed only under the assumption that methanol was formed in equimolar amounts with another C₁-containing component (product Y), which could not be analyzed separately with the micro-gas chromatograph.

The reaction rate is expressed either in terms of the acetonitrile formation rate per gram of zeolite per second or in terms of the turnover frequency per single Co atom (TOF, s⁻¹). Carbon selectivity (S_{C_i}) to a carbon-containing product, P_i , and nitro-

Table 2
Etching conditions and surface roughness of the TAMo substrates

TAMo substrate ^a	Conditions		Surface parameters	
	T (°C)	t (s)	R_a (nm)	Δw (g m ⁻²)
S ₀	–	–	13 ± 2	0
S ₄	50	30	14 ± 5	4
S ₅₅	70	60	45 ± 9	55
S ₁₂₀	80	120	90 ± 8	120

^a The subscript indicates the specific weight loss Δw of the Mo substrate after the etching treatment with a mixture of 4.3 vol% H₂O₂ (Fluka) and 3.6 vol% NH₄OH (Riedel de Haën) in distilled water.

gen selectivity (S_{N_j}) to a nitrogen-containing product, P_j , are defined as

$$S_{C_i} = \frac{y_{C_i} \cdot n_{C_i}}{\sum_i y_{C_i} \cdot n_{C_i}} \cdot 100\% \quad (3)$$

and

$$S_{N_j} = \frac{y_{N_j} \cdot m_{N_j}}{\sum_j y_{N_j} \cdot m_{N_j}} \cdot 100\%, \quad (4)$$

where y_{C_i} and y_{N_j} are the molar fractions and n_{C_i} and m_{N_j} are the number of carbon and nitrogen atoms in the product molecule, respectively.

3. Results and discussion

3.1. Effect of surface roughness on coverage

The surface roughness of the substrate was increased by a chemical etching procedure (Table 2). LSCM scans of the TAMo substrates (S₀, S₄, S₅₅, and S₁₂₀) before the synthesis are shown in Figs. 2a, 2c, 2e, and 2g. The corresponding SEM images of the as-synthesized zeolite Beta coatings are shown in Figs. 2b, 2d, 2f, and 2h. After the synthesis, uncovered areas remained on the nontreated substrate S₀, which has a constant waviness profile obtained in a roll-casting process. A closed layer of zeolite Beta crystals was obtained on S₄, which has

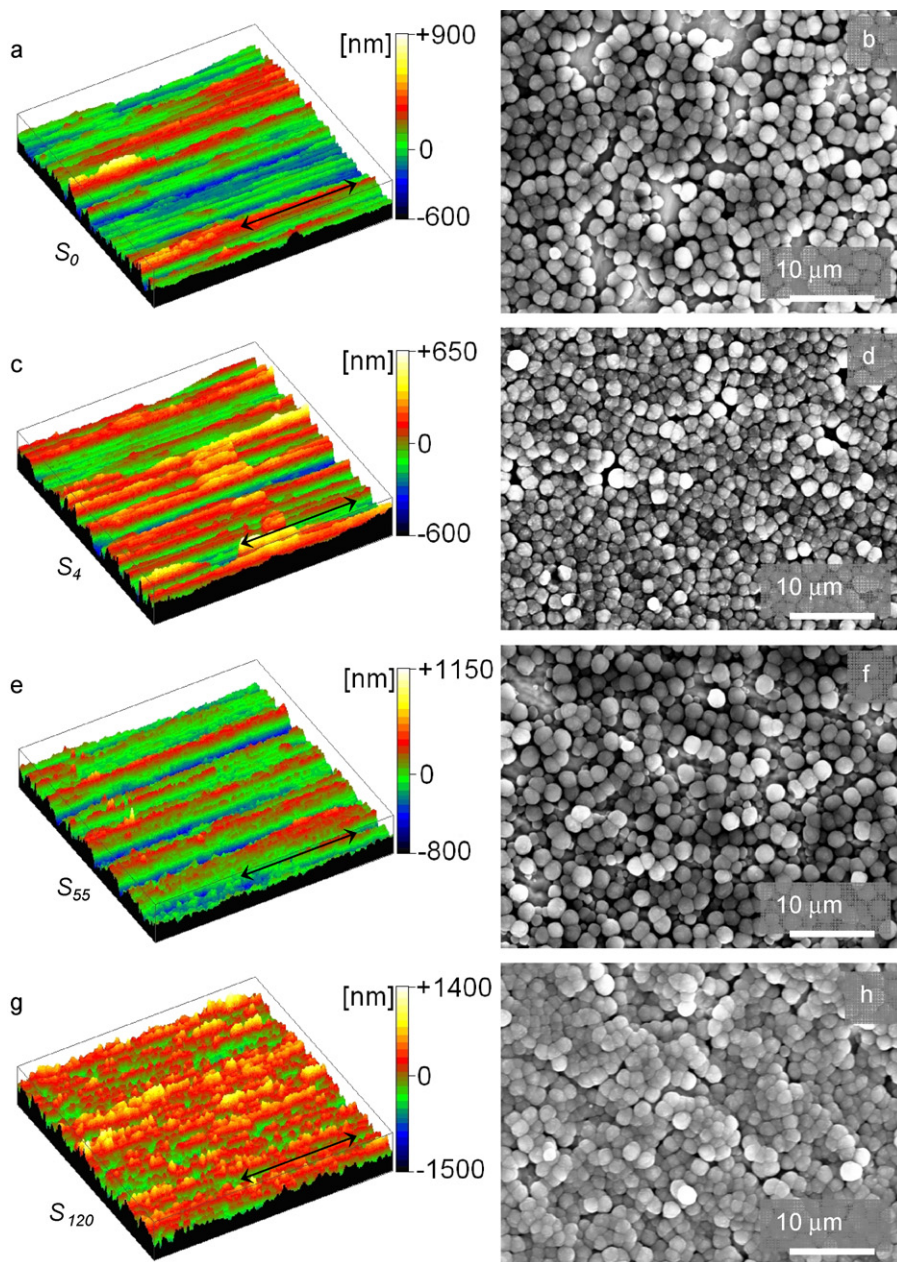


Fig. 2. LSCM scans (scan area is $320 \times 320 \mu\text{m}^2$) of the TAMo substrates: (a) S_0 , (c) S_4 , (e) S_{55} , and (g) S_{120} (Table 1) and the corresponding scanning electron micrographs of the as synthesized zeolite Beta coatings (b, d, f, and h, respectively). The black arrows in the LSCM scans indicate the direction of the lay of the Mo substrate parallel to which the 2D height profiles were digitized for the determination of the R_a value. Synthesis conditions: $T = 150^\circ\text{C}$, $t = 30$ h, initial heating rate = $10^\circ\text{C min}^{-1}$.

a similar surface roughness but a different surface morphology. Substrate S_4 was modified by a mild etching treatment only at the nanoscale level, which does not influence R_a (Fig. 1c). The zeolite coverage was increased by 35%, which is attributed to the increased number of surface irregularities. It was shown that formation of silicalite-1 and zeolite Y was improved on a plastically deformed or mechanically destroyed copper substrate because of the higher number of surface imperfections, which are supposed to be nucleation centers for zeolite crystals [31, 32]. It is expected that surface irregularities are far more homogeneously distributed over the surface after chemical etching compared with a mechanical surface treatment. Compared to

S_0 , S_4 has also a higher surface energy, which is favorable for anchoring of small crystals. The average diameter of zeolite crystals is $1.5 \mu\text{m}$. It is characteristic of S_0 and S_4 morphology that the difference in altitude between the highest and lowest points amounts to $1.3 \mu\text{m}$ in the direction perpendicular to lay. This is less than the mean diameter of a zeolite crystal of $1.5 \mu\text{m}$ (see Fig. 3a).

Substrates S_{55} and S_{120} were subjected to more severe etching treatments (Table 2), which resulted in an increased surface roughness (Figs. 2e and 2g). For S_{55} and S_{120} , the maximum difference between the top and bottom part of the substrate surface of 2.0 and $2.9 \mu\text{m}$, respectively, is larger than the average

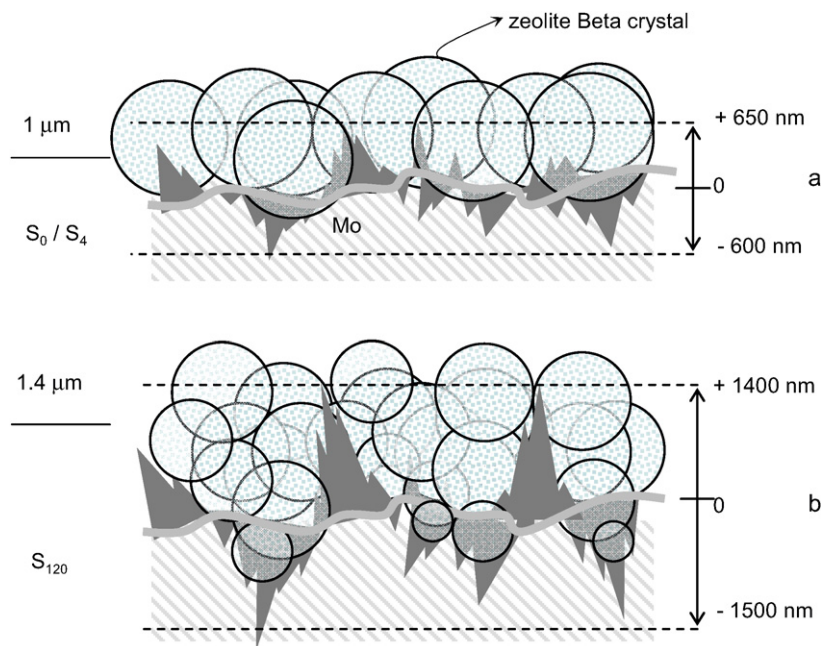


Fig. 3. Illustrations of the cross sections of the two-dimensional surface profiles of the zeolite Beta coatings on a Mo substrate. Panel (a) shows the surface profile of the substrates S_0 or S_4 , on which a single layer of zeolite Beta crystals (average crystal size is $1.5 \mu\text{m}$) are visible (compare (a) with Figs. 2a–2d). Panel (b) shows the surface profile of substrate S_{120} (Table 2) with a R_a value of 90 nm , consisting of large pockets in which zeolite Beta crystals can be deposited on top of each other (compare (b) with Figs. 2g and 2h).

diameter of the zeolite crystals. Therefore, the second layer of zeolite crystals can be deposited on top of the crystals located in the substrate pockets, as shown schematically in Fig. 3b. Thus, to obtain a single layer of zeolite crystals, the surface morphology has to contain numerous imperfections, while the available pockets should not exceed the size of the crystals.

3.2. Effect of surface hydrophilicity on coverage

The alumina and titania films were successively deposited by ALD [27,48]. The inner alumina film consists of a non-porous amorphous phase, which protects the substrate from oxidation in an oxygen-containing mixture [22]. No reflections from molybdenum oxides were observed in the XRD patterns of a Mo substrate coated with a 170-nm thin alumina film after 10 h in an air–water mixture at 550°C (Fig. 4b). The density of the alumina film of 3.5 g cm^{-3} is slightly lower than for $\alpha\text{-Al}_2\text{O}_3$ (3.97 g cm^{-3}), whereas their surface properties are reported to be similar [27]. Because the alumina film contains less than $1 \text{ OH group per nm}^2$ [33], an outer titania film was deposited to increase the surface wettability of the substrate [34].

The deposition temperature, film thickness, and nature of the titanium precursor (TiCl_4 and TiI_4) were varied to obtain an optimal hydrophilicity of the TiO_2 film after UV irradiation (Table 3). The difference between the thermal expansion coefficient of film and substrate must be as small as possible to avoid crack formation. For the same reason, thinner films are more preferred [49]. The highest temperature in the zeolite posttreatment is 500°C . Therefore, the ALD films should preferably be deposited at this temperature. Before the UV treatment, the

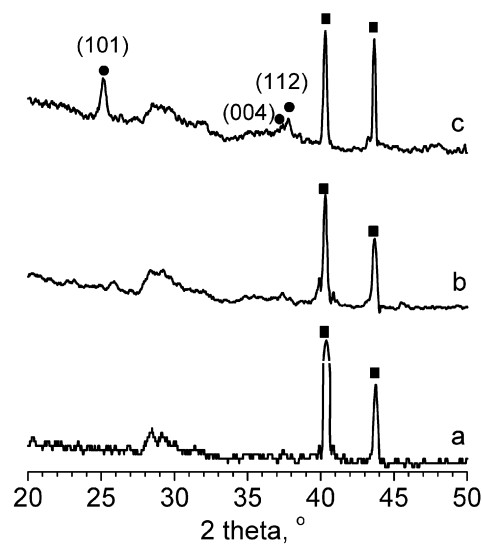


Fig. 4. XRD patterns of substrates after various surface modifications and treatments: (a) molybdenum (Mo) substrate, (b) Al_2O_3 (170 nm)/Mo substrate after 10 h of oxidation in an air/water ($2.3 \text{ vol}\%$) mixture at 550°C , (c) TiO_2 (50 nm)/ Al_2O_3 (170 nm)/Mo substrate (TAMo substrate). The reflections Mo (■) and anatase TiO_2 (●) are of the crystalline phases for indicated in the figure.

lowest water contact angle of 44° was observed for a film of 50 nm deposited at 500°C from the TiCl_4 precursor. This film has a low density of surface OH groups because of thermal dehydroxylation of the surface, resulting in a rather hydrophobic surface at this temperature. After the UV irradiation, superhydrophilic behavior (contact angle $<5^\circ$) was observed for all samples. The films obtained from TiCl_4 at 300°C remained superhydrophilic for at least 200 min , whereas those obtained at

Table 3
ALD parameters and water contact angle on the S_0 substrate

Temperature (°C)	Thickness (nm)	Pretreatment/titania precursor/contact angle (°)					
		No UV		UV (min) ^a			
		TiCl ₄	TiI ₄	TiCl ₄	TiI ₄		
				10	200	10	200
300	50	59 ± 3	75 ± 4	<5 ^b	<5	<5	<5
	100	68 ± 9	69 ± 12	<5	<5	<5	9
500	50	44 ± 8	74 ± 9	<5 (<5)	<5 (9)	<5	28
	100	77 ± 7	78 ± 5	<5	6	<5	30

^a Time between UV treatment and contact angle analysis. The substrate was positioned perpendicular to the UV source. Values in the parentheses are given for the parallel orientation of the substrates relative to the UV source.

^b Contact angle values below 5° cannot be analyzed accurately.

500 °C showed a slight increase of the contact angle. One may conclude that the deposition temperature and the film thickness do not influence the performance of the films obtained in the TiCl₄-H₂O ALD process. However, the films obtained from TiI₄ became much more hydrophobic, especially those deposited at 500 °C. This may be due to the different structure of the films. Both hydroxyl groups and chlorine ions can be easily incorporated in the film structure when TiCl₄ is used as a metal precursor. The TiI₄ process is faster than the TiCl₄ process, due to relatively easy ligand release at temperatures above 300 °C. Therefore, the TiI₄ process produces films with a higher degree of epitaxy and with a lower content of the bulk OH groups; however, the uniform films obtained in the TiI₄ process show a fast decay in hydrophilicity. This effect is especially pronounced at 500 °C. Therefore, TiCl₄ was chosen as an ALD precursor for deposition of 50-nm titania films at 500 °C. At these conditions, the anatase structure with the (101) plane as the predominant plane of crystallization has been identified as the main phase (Fig. 4c). The anatase structure was also obtained on a silicon substrate at a deposition temperature of 500 °C [48]. However, minor phases of rutile may be present, which could not be identified due to the thin (50-nm) layer.

The growth of zeolite Beta coatings at 150 °C is remarkably enhanced by the superhydrophilicity of the TAMo substrate. A TAMo substrate without UV irradiation has a coverage of ca. 50% of a single crystal layer (Fig. 5a), whereas the UV-irradiated substrate was completely covered with a single layer of zeolite Beta crystals after a synthesis time of 16 h (Fig. 5b). The increased hydrophilicity of the substrate resulted in a better compatibility with the precursor gel. The zeolite crystals in the coating evolved from an amorphous gel layer, which was initially attached to the surface of the substrate [47]. The gel phase is still partly visible in Fig. 5b. Zeolite Beta crystals were firmly attached to the substrate due to the increased number of defect sites and hydroxyl groups on the TiO₂ surface. This clearly demonstrates that the wettability of the surface of the TAMo substrates influenced the zeolite Beta coating properties. Similar findings were reported in a study on the improvement of zeolite NaA nucleation sites on (001) rutile by means of UV radiation [34].

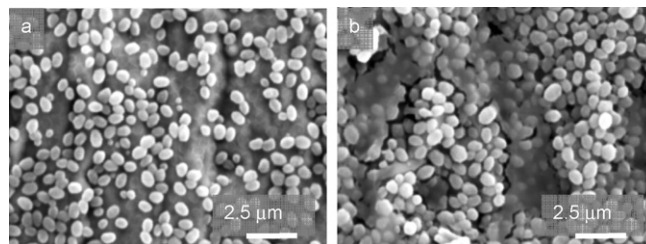


Fig. 5. Scanning electron micrographs of zeolite Beta coatings without (a) and after (b) a UV irradiation of the S_{55} substrate. Synthesis conditions: $T = 150^\circ\text{C}$, $t = 16$ h, initial heating rate = 1°C min^{-1} .

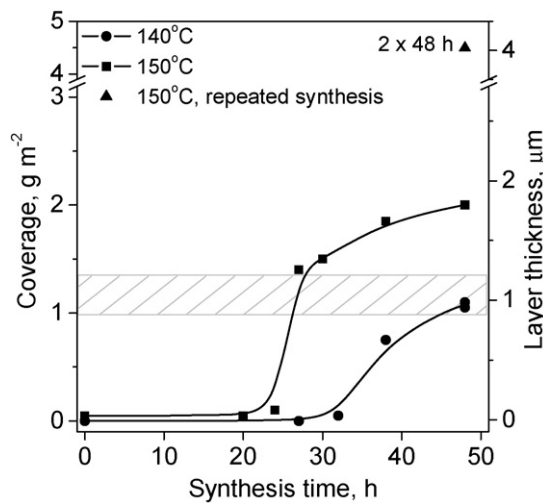


Fig. 6. Zeolite Beta coverage and average layer thickness of the coatings (a.s.) obtained on substrate S_4 as a function of synthesis time at 140 and 150 °C. Heating rate: $10^\circ\text{C min}^{-1}$. The shaded area indicates the coverage of a single layer of zeolite Beta crystals. Also the coverage after a repeated synthesis (\blacktriangle , 2×48 h) is shown.

3.3. In situ synthesis of a single layer of zeolite Beta crystals

The crystallization of zeolite Beta takes from 20 h to several weeks, depending on the synthesis conditions [47,50–52]. Zeolite Beta was obtained after 20 h from a Na-, K-, and TEOH-containing precursor gel with a SiO₂/Al₂O₃ ratio of 50 and a temperature of 135 °C [51]. Therefore, this recipe was taken as a good starting point for further optimization. In this study, the synthesis temperature was increased to 140 or 150 °C, and silica sol was used as a reactive silica source to obtain higher nucleation and crystallization rates.

A single layer of zeolite Beta crystals on substrate S_4 corresponds to a zeolite coverage between 1.0 and 1.3 g m⁻² depending on the average crystal size. A single layer of zeolite Beta crystals was obtained after 48 and 26 h at 140 and 150 °C, respectively (Fig. 6). Correspondingly, the induction period decreased from 30 to 24 h. Increasing the reaction temperature from 140 to 150 °C caused an increase in the crystallization rate, along with a simultaneous increase in the average crystal size from 0.82 (Fig. 7a) to 1.57 μm (Fig. 7b), while a narrow unimodal crystal size distribution (CSD) was preserved. The narrow CSD indicates that the crystals were grown from a gel layer initially deposited at the substrate surface. Initially, all

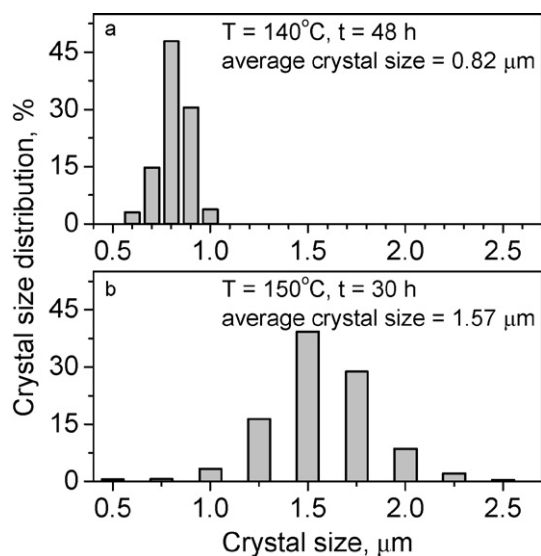


Fig. 7. Crystal size distribution of zeolite Beta coatings obtained on substrate S_4 at (a) 140 °C after 48 h, and (b) 150 °C after 30 h corresponding to the SEM images of Figs. 9a and 9c. The synthesis conditions are the same as those in Fig. 6.

crystals grew fast due to the very high concentration of nutrients in both the gel layer and the liquid phase. The crystal growth rate reduced rapidly as the concentrations of nutrients were depleted in the gel layer in the course of crystallization. Therefore, zeolite crystals with the same size at the end of the crystallization could be formed at different nucleation times and pass different crystal growth periods [47]. The zeolite Beta crystal size can be further decreased by a reduction in both the temperature of crystallization [50] and the concentration of alkali cations, especially potassium [53].

Figs. 8a and 8c show SEM images of the zeolite Beta coatings obtained at 140 and 150 °C after 48 h and 30 h, respectively. The SEM inset (Fig. 8a) and the AFM scan (Fig. 8b) show the perfectly closed single layer of well-arranged zeolite Beta crystals on the TAMo substrate at 140 °C. A time interval of just 2 h (between 25 and 27 h of synthesis) corresponds to a single layer of crystals ($1\text{--}1.3\text{ g m}^{-2}$) at 150 °C (Fig. 6). After 30 h, some crystals were already present on top of the coating (Fig. 8c). Moreover, after rapid heating (10 °C min^{-1}) of the synthesis mixture at 150 °C, the zeolite Beta coating consisted of two layers [48]. The inner layer, comprising relatively small crystals, was grown directly on the surface at the substrate/gel interface, whereas the visible outer layer of larger crystals was crystallized into the gel layer starting from the gel-liquid interface. The AFM scan (Fig. 8d) shows a rougher coating morphology compared with the coating obtained at 140 °C (Fig. 8b). The crystal shape seems independent on the reaction temperature. At both temperatures, the crystals do not have a well-defined crystal habit, but appear round-shaped. Some sharp edges or terraces can be observed on the large zeolite Beta crystals obtained at 150 °C. The zeolite Beta coating thickness could be increased by up to approximately 4 μm by repeating the synthesis procedure at 150 °C (Fig. 6). A continuous coating with a rough morphology was obtained (Fig. 9a). The SEM image in Fig. 9b shows the cross-section of the coating.

Zeolite Beta was the only crystalline phase present in the coatings. Some selected XRD results of the coatings are presented in Figs. 10d–10f. The XRD patterns correspond well with the reference patterns of as-synthesized and calcined zeolite Beta powder (Figs. 10a and 10b) obtained from a similar precursor gel composition as used in this study [43]. Crystallographic faulting is often observed in the zeolite Beta struc-

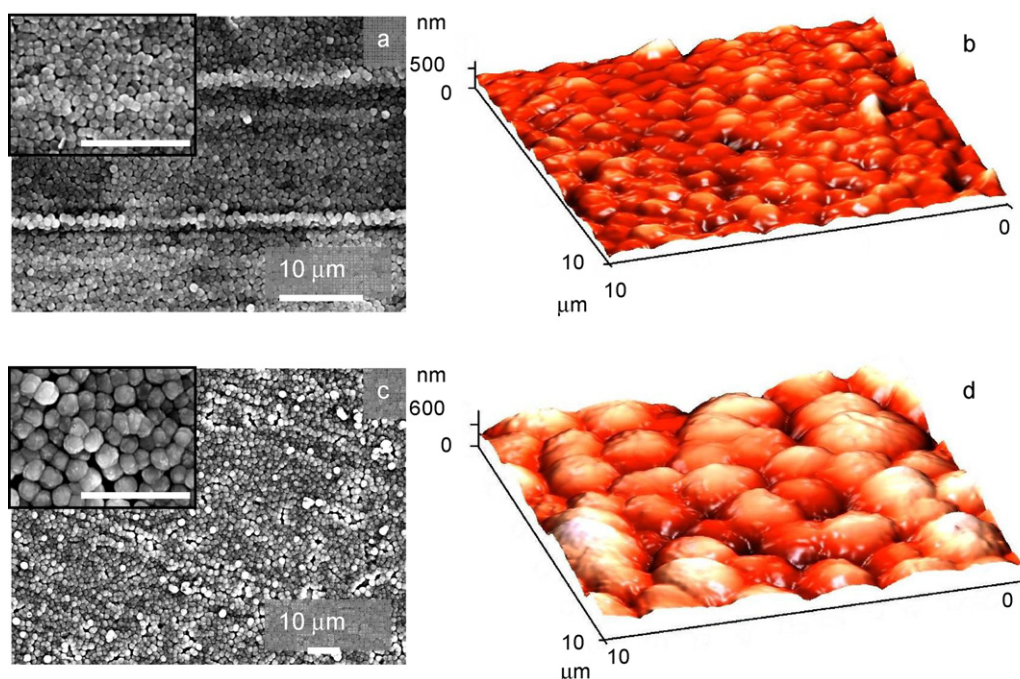


Fig. 8. Scanning electron micrographs (a and c) and the corresponding AFM scans (scan area is $10 \times 10\text{ }\mu\text{m}^2$) (b and d) of zeolite Beta coatings (a.s.) obtained on substrate S_4 at 140 °C after 48 h (a and b), and 150 °C after 30 h (c and d). Close-up SEM images of the coatings are shown in the insets (scale bar indicates 10 μm). The synthesis conditions are the same as those in Fig. 6.

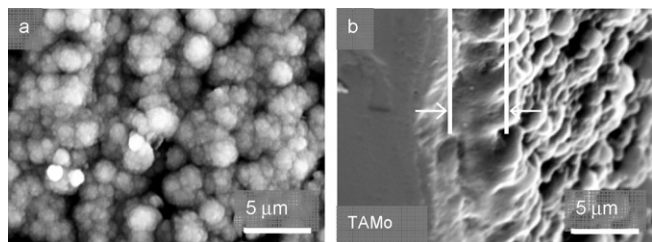


Fig. 9. Scanning electron micrographs of (a) the surface and (b) (tilting angle = 75°) the cross section of the zeolite Beta coating obtained after a repeated synthesis at 150 °C (see also Fig. 6). The layer thickness of the coating is 4 μm. The synthesis conditions are the same as those in Fig. 6.

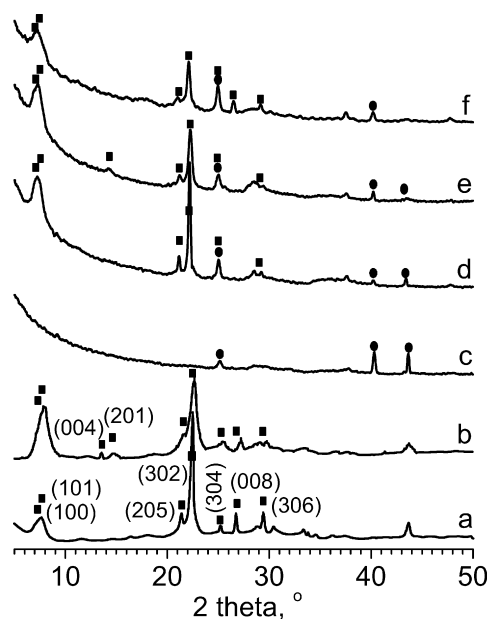


Fig. 10. Reference XRD patterns of (a) as synthesized zeolite Beta powder [54] and (b) calcined zeolite Beta powder [54], and (c) of the TAMo substrate. XRD patterns of zeolite Beta coatings: (d) as synthesized, 150 °C, 48 h, (e) calcined, 150 °C, 48 h, and (f) repeated synthesis, as synthesized, 140 °C, 48 h.

ture [2]. The broad peaks from both the (100) and (101) reflections in the 6–8° 2θ range indicates that polymorphs A and B are approximately equally distributed in the BEA structure [55, 56]. Along with the (100) and (101) reflections, the XRD patterns from the coatings contain strong reflections, with (hkl) values equal to (205), (302), (304), and (306). The zeolite Beta crystals in the coating have a preferred orientation, because the reflections from the crystallographic planes parallel to the crystallographic c -axis are not present in the XRD pattern (cf. the XRD patterns in Figs. 10a and 10d of as-synthesized zeolite Beta powder and coating, respectively), whereas the (201) reflection is clearly visible (cf. the XRD patterns in Figs. 10b and 10e of calcined zeolite Beta powder and coating, respectively). A repeated synthesis at 140 °C resulted in a multilayer of zeolite Beta crystals. Fig. 10f shows the XRD pattern of this as-synthesized coating, in which the (008) reflection is visible. Apparently, the preferred orientation of crystals disappears when they grow or are deposited on top of the first layer of crystals on the TAMo substrate.

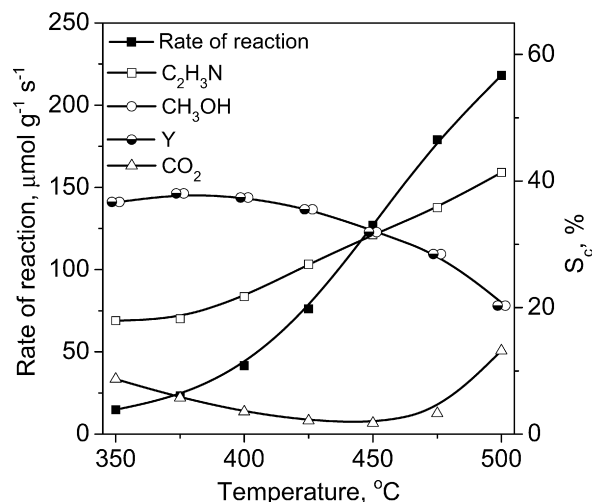
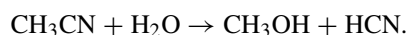


Fig. 11. Activity and product selectivity of the Co-Beta coating (Si/Al = 21, Co/Al = 0.5) as a function of the reaction temperature. Product Y denotes a C₁ containing product, most likely HCN. The coatings were tested at a total flow rate of 33 mL min⁻¹ (STP) consisting of 2 vol% of ethylene, 2 vol% ammonia and 2 vol% oxygen, He-balance.

3.4. Activity of Co-Beta coatings in ethylene ammoxidation

Co-Beta coatings were prepared from the as-synthesized coatings with a Si/Al ratio of 23 through a series of calcination and ion-exchange treatments (Table 1). A Co/Al ratio of 0.5 was obtained in the coatings after ion exchange with 10⁻⁴ M aqueous cobalt acetate solution. The Co-zeolite Beta coatings were tested in a microstructured reactor in a highly exothermic ethylene ammoxidation. A maximum rate of acetonitrile formation of 220 μmol g⁻¹ s⁻¹ was reached at 500 °C (Fig. 11). Bare Co²⁺ cations, balanced by two adjacent aluminum atoms in the zeolite framework, are the most active sites in the ammoxidation process [57,58]. Thus, higher rates of reaction can be obtained by increasing the aluminium content in the zeolite framework. At a Si/Al ratio of 23, the number of aluminium pairs in the zeolite Beta topology was 30% of the total number of aluminium atoms; at a Si/Al ratio of 13, this value was 80% [59,60].

The highest carbon-selectivity (S_C) to acetonitrile was only 42%, which is two times lower than that reported over Co-Beta pelletized catalysts with a Si/Al ratio of 12 [62]. Furthermore, methanol was formed on the coatings with a selectivity of 20% at 500 °C but was not a product on pelletized Co-Beta catalysts. In the presence of water, methanol can be formed on two adjacent bivalent cations [63],



A constant N-selectivity (S_N) to nitrogen of 80% was obtained, confirming the selective oxidation of ammonia under the applied reaction conditions. Recently, we showed that higher reaction rates indeed were obtained over Co-Beta coatings with a Si/Al ratio of 15 compared with Co-Beta pelletized catalysts, due to the absence of transport limitations in the coatings [61].

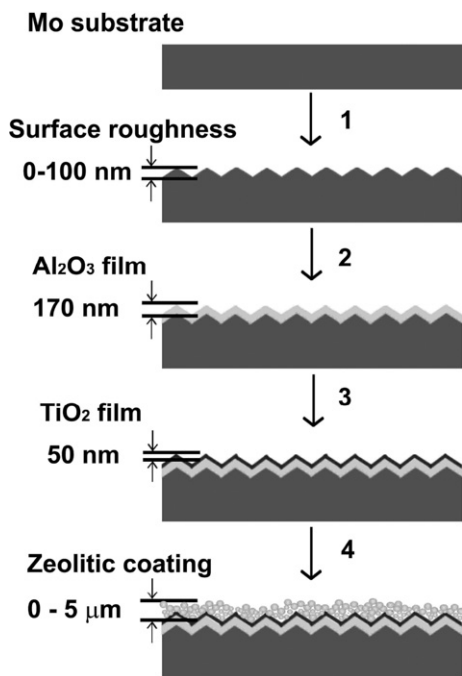


Fig. 12. Method for the in situ synthesis of zeolitic coatings. Surface modification of the molybdenum (Mo) substrate: (1) cleaning and etching of the substrate, (2) deposition of a 170 nm Al_2O_3 film by atomic layer deposition (ALD), (3) deposition of a 50 nm TiO_2 film by ALD. Step (4) illustrates the in situ crystallization process of zeolitic coatings on the TAMo substrate (after a UV treatment of the TiO_2 surface).

4. Conclusion

A method has been developed for the in situ synthesis of zeolitic coatings on a metal substrate for application in a microstructured reactor. The method is exemplified in Fig. 12 for the in situ growth of a single layer of zeolite Beta crystals on a molybdenum substrate. First, the number of surface irregularities on the substrate was increased by a chemical etching procedure (step 1) to enhance both the number of nucleation sites and the positions of zeolite crystals for anchoring. For a single layer of zeolite Beta crystals 0.5–1.5 μm in size, a low surface roughness (14 nm) was required. Then, two thin films of Al_2O_3 (170 nm, step 2) and TiO_2 (50 nm, step 3) were successively deposited by ALD on the substrate. The internal Al_2O_3 film protects the Mo substrate from oxidation up to 550 °C in an oxidative environment. High wettability of the external TiO_2 film after UV irradiation increases zeolite nucleation at its surface. A stable superhydrophilic TiO_2 surface (water contact angle below 5°) for at least 200 min was obtained after deposition of a 50 nm film at 500 °C from a TiCl_4 precursor. A perfectly ordered single layer of zeolite Beta crystals was obtained from a viscous Na, K, and TEAOH precursor gel with a $\text{SiO}_2/\text{Al}_2\text{O}_3$ ratio of 46 at a synthesis temperature of 140 °C after 48 h (step 4).

The Co-Beta coatings ($\text{Si}/\text{Al} = 23$, $\text{Co}/\text{Al} = 0.5$) were tested in the ammoxidation of ethylene to acetonitrile in a microstructured reactor. A maximum rate of reaction of 220 $\mu\text{mol C}_2\text{H}_3\text{N g}^{-1} \text{s}^{-1}$ was obtained at 500 °C, with a carbon selectivity to acetonitrile of 42%. Higher rates of reaction can be

obtained when the aluminum content in the zeolite Beta coating is increased.

Acknowledgments

This work was supported by the Dutch Technology Foundation (STW, project no. EPC.5543), Shell International Chemicals B.V., Akzo Nobel Chemicals B.V., and Avantium Technologies B.V. The authors thank Dr. Milja Mäkelä of Nanoscale Oy (Finland) for assistance with the development of the ALD procedure, and Dr. Denis Ovchinnikov for assistance with the atomic force microscopy.

References

- [1] M. Stöcker, *Microporous Mesoporous Mater.* 82 (2005) 257.
- [2] J.C. Jansen, E.J. Creyghton, S.L. Njo, H. van Koningsveld, H. van Bekkum, *Catal. Today* 38 (1997) 205.
- [3] D.E. de Vos, P.A. Jacobs, *Microporous Mesoporous Mater.* 82 (2005) 293.
- [4] A. de Lucas, M.J. Ramos, F. Dorado, P. Sánchez, J.L. Valverde, *Appl. Catal. A* 289 (2005) 205.
- [5] Z.-W. Liu, X. Li, K. Asami, K. Fujimoto, *Appl. Catal. A* 300 (2006) 162.
- [6] H.-H. Chen, S.-C. Shen, X. Chen, S. Kawi, *Appl. Catal. B* 50 (2004) 37.
- [7] A.P. Ferreira, C. Henriques, M.F. Ribeiro, F.R. Ribeiro, *Catal. Today* 107–108 (2005) 181.
- [8] E. Creyghton, Ph.D. thesis, Delft University of Technology, 1996.
- [9] M. Lashdaf, V.-V. Nieminen, M. Tiitta, T. Venäläinen, H. Österholm, O. Krause, *Microporous Mesoporous Mater.* 75 (2004) 149.
- [10] Y. Li, J.N. Armor, *J. Catal.* 173 (1998) 511.
- [11] J. Hedlund, O. Öhrman, V. Msimang, E. van Steen, W. Böhringer, S. Sibya, K. Möller, *Chem. Eng. Sci.* 59 (2004) 2647.
- [12] M. Torres, L. López, J.M. Domínguez, A. Mantilla, G. Ferrat, M. Gutierrez, M. Maubert, *Chem. Eng. J.* 92 (2003) 1.
- [13] O.L. Oudshoorn, M. Janissen, W.E.J. van Kooten, J.C. Jansen, H. van Bekkum, C.M. van den Bleek, H.P.A. Calis, *Chem. Eng. J.* 54 (1999) 1413.
- [14] N. van der Puil, F.M. Dautzenberg, H. van Bekkum, J.C. Jansen, *Microporous Mesoporous Mater.* 27 (1999) 95.
- [15] L. Li, B. Xue, J. Chen, N. Guan, F. Zhang, D. Liu, H. Feng, *Appl. Catal. A* 292 (2005) 312.
- [16] A.E.W. Beers, T.A. Nijhuis, N. Aalders, F. Kapteijn, J.A. Moulijn, *Appl. Catal. A* 243 (2003) 237.
- [17] A. Bueno-López, D. Lozano-Castelló, I. Such-Basáñez, J.M. García-Cortés, M.J. Illán-Gómez, C. Salinas-Martínez de Lecea, *Appl. Catal. B* 58 (2005) 1.
- [18] E.V. Rebrov, G.B.F. Seijger, H.P.A. Calis, M.H.J.M. de Croon, C.M. van den Bleek, J.C. Schouten, *Appl. Catal. A* 206 (2001) 125.
- [19] J. Coronas, J. Santamaria, *Chem. Eng. Sci.* 59 (2004) 4879.
- [20] J.C.M. Muller, G. Hakvoort, J.C. Jansen, *J. Therm. Anal.* 53 (1998) 449.
- [21] Y. Shan, S. Wan, J.L.H. Chau, A. Gavriilidis, K.L. Yeung, *Microporous Mesoporous Mater.* 42 (2001) 157.
- [22] M.J.M. Mies, E.V. Rebrov, M.H.J.M. de Croon, J.C. Schouten, *Chem. Eng. J.* 101 (2004) 225.
- [23] M.J.M. Mies, J.L.P. van den Bosch, E.V. Rebrov, J.C. Jansen, M.H.J.M. de Croon, J.C. Schouten, *Catal. Today* 110 (2005) 38.
- [24] E.V. Rebrov, M.H.J.M. de Croon, J.C. Schouten, *Book of Abstracts of 7th European Conference on Catalysis, EuropaCat VII, August 28–September 1, 2005, Sofia, Bulgaria* (2005), p. 321.
- [25] S.A. Kuznetsov, S.V. Kuznetsova, E.V. Rebrov, M.J.M. Mies, M.J.H.M. de Croon, J.C. Schouten, *Surf. Coat. Technol.* 195 (2005) 182.
- [26] S.A. Kuznetsov, E.V. Rebrov, M.J.M. Mies, M.H.J.M. de Croon, J.C. Schouten, *Surf. Coat. Technol.* 201 (2006) 971.
- [27] M.D. Groner, J.W. Elam, F.H. Fabreguette, S.M. George, *Thin Solid Films* 413 (2002) 186.
- [28] N.D. Hoivik, J.W. Elam, R.J. Linderman, V.M. Bright, S.M. George, Y.C. Lee, *Sens. Actuators A* 103 (2003) 100.

- [29] J.C. Jansen, W. Nugroho, H. van Bekkum, in: R. Von Ballmoos, J.B. Higgins, M.M.J. Treacy (Eds.), Proceedings of the 9th International Zeolite Conference, Montreal, 5–10 July 1992, p. 247.
- [30] Z. Wang, Y. Yan, *Microporous Mesoporous Mater.* 48 (2001) 229.
- [31] V. Valtchev, S. Mintova, L. Konstantinov, *Zeolites* 15 (1995) 679.
- [32] V. Valtchev, S. Mintova, *Zeolites* 15 (1995) 171.
- [33] J.C. Jansen, J.H. Koegler, H. van Bekkum, H.P.A. Calis, C.M. van den Bleek, F. Kapteijn, J.A. Moulijn, E.R. Geus, N. Van der Puil, *Microporous Mesoporous Mater.* 21 (1998) 213.
- [34] A.W.C. van den Berg, L. Gora, J.C. Jansen, T. Maschmeyer, *Microporous Mesoporous Mater.* 66 (2003) 303.
- [35] L. Sirghi, Y. Hatanaka, *Surf. Sci.* 530 (2003) 323.
- [36] X. Wang, Y. Yu, X. Hu, L. Gao, *Thin Solid Films* 371 (2000) 148.
- [37] J. Aarik, A. Aidla, T. Uustare, V. Sammelselg, *J. Cryst. Growth* 148 (1995) 268.
- [38] J. Aarik, A. Aidla, V. Sammelselg, T. Uustare, *J. Cryst. Growth* 181 (1997) 259.
- [39] J. Aarik, A. Aidla, H. Mändar, T. Uustare, *Appl. Surf. Sci.* 172 (2001) 148.
- [40] D.R.G. Mitchell, D.J. Attard, G. Triani, *Thin Solid Films* 441 (2003) 85.
- [41] D.R.G. Mitchell, G. Triani, D.J. Attard, K.S. Finnie, P.J. Evans, C.J. Barbé, J.R. Bartlett, *Device and Process Technologies for MEMS, Microelectronics and Photonics III*, in: J.C. Chiao, A.J. Hariz, D.N. Jamieson, G. Parish, V.K. Varadan (Eds.), in: Proceedings of the SPIE, vol. 5276, 2004, p. 296.
- [42] M. Schuisky, A. Härsta, A. Aidla, K. Kukli, A.-A. Kiisler, J. Aarik, *J. Electrochem. Soc.* 147 (2000) 3319.
- [43] D.R.G. Mitchell, D.J. Attard, G. Triani, *J. Cryst. Growth* 285 (2005) 208.
- [44] K. Kukli, A. Aidla, J. Aarik, M. Schuisky, A. Härsta, M. Ritala, M. Leskelä, *Langmuir* 16 (2000) 8122.
- [45] M. Schuisky, J. Aarik, K. Kukli, A. Aidla, A. Härsta, *Langmuir* 17 (2001) 5508.
- [46] M. Schuisky, K. Kukli, J. Aarik, J. Lu, A. Härsta, *J. Cryst. Growth* 235 (2002) 293.
- [47] M.J.M. Mies, E.V. Rebrov, J.C. Jansen, M.H.J.M. de Croon, J.C. Schouten, *Microporous Mesoporous Mater.* (2007), <http://dx.doi.org/10.1016/j.micromeso.2007.02.032>.
- [48] M. Ritala, M. Leskelä, E. Nykänen, P. Soininen, L. Niinistö, *Thin Solid Films* 225 (1993) 288.
- [49] G. Krautheim, T. Hecht, S. Jakschik, U. Schröder, W. Zahn, *Appl. Surf. Sci.* 252 (2005) 200.
- [50] J. Pérez-Pariente, J.A. Martens, P.A. Jacobs, *Zeolites* 8 (1988) 46.
- [51] M.A. Cambor, A. Mifsud, J. Pérez-Pariente, *Zeolites* 11 (1991) 792.
- [52] R.L. Wadlinger, G.T. Kerr, E.J. Rosinski, U.S. Patent 3,308,069 (1967).
- [53] M.A. Cambor, J. Pérez-Pariente, *Zeolites* 11 (1991) 202.
- [54] H. Robson, *Microporous Mater.* 22 (1998) 551.
- [55] M.M.J. Treacy, J.B. Higgins, R. von Ballmoos, *Zeolites* 16 (1996) 323.
- [56] B.J. Schoeman, E. Babouchkina, S. Mintova, V.P. Valtchev, *J. Stereol. Porous Mater.* 8 (2001) 13.
- [57] R. Bulánek, K. Novoveská, B. Wichterlová, *Appl. Catal. A* 235 (2002) 181.
- [58] J. Dědeček, D. Kaucý, B. Wichterlová, *Microporous Mesoporous Mater.* 35–36 (2000) 483.
- [59] O. Bortnovsky, Z. Sobalík, B. Wichterlová, *Microporous Mesoporous Mater.* 46 (2001) 265.
- [60] B. Wichterlová, J. Dědeček, Z. Sobalík, J. Čejka, *Stud. Surf. Sci. Catal.* 135 (2001).
- [61] M.J.M. Mies, E.V. Rebrov, C.J.B.U. Schiepers, M.H.J.M. de Croon, J.C. Schouten, *Chem. Eng. J. Chem. Eng. Sci.* (2007), <http://dx.doi.org/10.1016/j.ces.2006.12.018>.
- [62] Y. Li, J.N. Armor, *J. Catal.* 173 (1998) 511.
- [63] T. Lu, X. Zhuang, Y. Li, S. Chen, *J. Am. Chem. Soc.* 126 (2004) 4760.